Hydrological Processes

WILEY

RESEARCH ARTICLE OPEN ACCESS

Energy-Water Asynchrony Principally Determines Water Available for Runoff From Snowmelt in Continental Montane Forests

Ryan William Webb[1] | John F. Knowles[2] | Alex Fox[3] | Alex Fabricus[1] | Timothy Corrie[4] | Kori Mooney[1] | Jocelyn Gallais[1] | Nana Afua Gyau Frimpong[1] | Christopher Akuka Akurugu[5] | Greg Barron-Gafford[6] | Peter D. Blanken[7] | Sean P. Burns[7,8] | John Frank[9] | Marcy Litvak[10]

[1]Department of Civil & Architectural Engineering and Construction Management, University of Wyoming, Laramie, Wyoming, USA | [2]Department of Land Resources and Environmental Sciences, Montana State University, Bozeman, Montana, USA | [3]Department of Botany, University of Wyoming, Laramie, Wyoming, USA | [4]Department of Atmospheric Science, University of Wyoming, Laramie, Wyoming, USA | [5]Department of Geology & Geophysics, University of Wyoming, Laramie, Wyoming, USA | [6]School of Geography, Development & Environment, University of Arizona, Tucson, Arizona, USA | [7]Department of Geography, University of Colorado, Boulder, Colorado, USA | [8]NSF National Center for Atmospheric Research, Boulder, Colorado, USA | [9]Rocky Mountain Research Station, USDA Forest Service, Fort Collins, Colorado, USA | [10]Department of Biology, University of New Mexico, Albuquerque, New Mexico, USA

Correspondence: Ryan William Webb (ryan.webb@uwyo.edu)

Received: 20 February 2024 | **Revised:** 13 September 2024 | **Accepted:** 17 September 2024

Funding: This work was supported by the U.S. Department of Energy through the AmeriFlux Management Project at Lawrence Berkeley National Laboratory (#7542010), the USDA Forest Service, Rocky Mountain Research Station (GLE), and National Science Foundation EAR awards 0724958 and 1331408 to the Catalina-Jemez Critical Zone Observatory (MtB).

Keywords: eddy covariance | hydrologic partitioning | montane forest hydrology | snow hydrology | water available for runoff | water balance

ABSTRACT

Changes in the volume, rate, and timing of the snowmelt water pulse have profound implications for seasonal soil moisture, evapotranspiration (ET), groundwater recharge, and downstream water availability, especially in the context of climate change. Here, we present an empirical analysis of water available for runoff using five eddy covariance towers located in continental montane forests across a regional gradient of snow depth, precipitation seasonality, and aridity. We specifically investigated how energy-water asynchrony (i.e., snowmelt timing relative to atmospheric demand), surface water input intensity (rain and snowmelt), and observed winter ET (winter AET) impact multiple water balance metrics that determine water available for runoff (WAfR). Overall, we found that WAfR had the strongest relationship with energy-water asynchrony (adjusted $r^2 = 0.52$) and that winter AET was correlated to total water year evapotranspiration but not to other water balance metrics. Stepwise regression analysis demonstrated that none of the tested mechanisms were strongly related to the Budyko-type runoff anomaly (highest adjusted $r^2 = 0.21$). We, therefore, conclude that WAfR from continental montane forests is most sensitive to the degree of energy-water asynchrony that occurs. The results of this empirical study identify the physical mechanisms driving variability of WAfR in continental montane forests and are thus broadly relevant to the hydrologic management and modelling communities.

1 | Introduction

Runoff from snowmelt is critical to supporting communities and ecosystems globally (Adam, Hamlet, and Lettenmaier 2009; Bales et al. 2006; Mankin et al. 2015). In the western United States, local economies and water storage in reservoirs rely on runoff from mountain snowpacks (Li et al. 2017; Sturm, Goldstein, and Parr 2017). With increased winter season energy (Harpold

et al. 2012; Knowles, Dettinger, and Cayan 2006; Sexstone et al. 2018) and mountain snowpacks are projected to decrease in volume (Hale et al. 2023; Immerzeel et al. 2020) and melt earlier (Musselman et al. 2017) because of climate change, it is critical to fully constrain the impact of these changes. However, uncertainties remain with studies finding conflicting results in terms of total runoff volume (Gordon et al. 2022; Hammond and Kampf 2020; McCabe, Wolock, and Valentin 2018; Milly, Kam, and Dunne 2018; Vano et al. 2014). With runoff from seasonal snowpacks identified as one of the fastest-changing processes in hydrology (IPCC 2022), accurate water resource forecasting depends on a thorough understanding of the mechanisms driving variability in water available for runoff (WAfR).

Several mechanisms have been identified as contributors to changes in snowmelt-driven runoff (e.g., Gordon et al. 2022). A primary mechanism is winter vapour losses, mostly driven by sublimation that may increase in drier and/or windier conditions (Sexstone et al. 2018), reducing the volume of snow water equivalent (SWE) available for spring runoff (Gordon et al. 2022). A second mechanism is the snowmelt rate which will likely decrease in warmer conditions as snowmelt begins earlier in the year (Musselman et al. 2017), with the potential to reduce subsurface flow and subsequent system efficiency in producing WAfR (Barnhart et al. 2016). A third mechanism is the asynchrony between atmospheric energy demand and water input from snowmelt, with higher asynchrony lengthening the growing season which results in increased stress on vegetation (Hale et al. 2023), potentially reducing total WAfR (Immerzeel et al. 2020). However, there is no consensus on the impacts of these mechanisms individually on water availability for downstream communities (Gordon et al. 2022).

Many previous studies that investigated snowmelt runoff dynamics were based on hydrologic models (e.g., Barnhart et al. 2016; Gordon et al. 2022; Hale et al. 2023). However, hydrologic modelling frameworks may contribute to uncertainty when model structures do not properly represent snowmelt dynamics (e.g., Webb et al. 2022). Hydrologic model structures include assumptions to solve the complex sets of equations within each model. One common assumption is to apply a static air temperature for partitioning rain and snow, which involves a complex set of processes and can occur at a range of air temperatures (Jennings et al. 2018). Additionally, snow surface temperature is difficult to accurately simulate in hydrologic models but can significantly impact snow-atmosphere energy and vapour exchange (Raleigh et al. 2013). Furthermore, hydrologic models may lack the structure to represent some of the primary runoff mechanisms transporting snowmelt water to streams in mountain watersheds (Webb et al. 2022), or assume no change in interannual watershed storage that is not accurate in many mountain environments (Brooks et al. 2021; Knowles et al. 2015). Therefore, while these assumptions are necessary for modelling, it is important to ensure that simulations are complemented with empirical studies to ensure that important physical mechanisms are properly represented as intended for any future projections (Kirchner 2006).

Forested areas contribute nearly half of the North American snowpack storage (Kim et al. 2021), the goal of this study is to advance understanding of the physical mechanisms that affect ecosystem scale WAfR variability in mid-latitude, continental montane environments. The analysis was performed using empirical data to mechanistically investigate relationships between WAfR metrics and: (1) energy-water asynchrony, (2) the intensity of surface water input (SWI), and (3) winter season evapotranspiration; these physical processes represent changes to the volume of snow, the rate of melt, and the timing of melt, respectively.

2 | Data and Methods

2.1 | Sites and Data Description

Five AmeriFlux sites were selected to represent ecosystem-scale dynamics (e.g., Running et al. 1999) along an approximate north–south transect of continental montane environments in the contiguous U.S. (Figure 1): GLEES in southeastern Wyoming (GLE; Frank and Massman 2021); Niwot Ridge in northern Colorado (NR1; Blanken et al. 2022); Valles Caldera Mixed Conifer in northern New Mexico (Vcm; Litvak 2023b); Mountainaire pinyon-juniper in central New Mexico (Mpj; Litvak 2023a); and Mt. Bigelow in southeastern Arizona (MtB; Barron-Gafford 2022). These sites are located across a hydroclimatic gradient (i.e., colder/wetter in the north and warmer/drier in the south), but all sites receive snowfall, with observed peak annual snow depths ranging from 14 to 280 cm and snowfall making up approximately 10% to 80% of total annual precipitation. Available data from the 2014–2022 water years were utilised for analysis due to prior disturbances at two sites, beetle kill at GLE from 2008 to 2010 and a stand-replacing fire at Vcm in 2013. The southern and/or disturbed sites also represent potential future conditions at the northern/undisturbed sites (e.g., Knowles et al. 2020). All sites are situated at elevations above 2000 m a.s.l. and have at least seven water years (October 1–September 30) of data. In total, 39 water years of data were used for analysis. The hydroclimate of these 39 water years included 11 water years with total precipitation larger than 10% above the site mean, 11 with total precipitation less than 10% below the site mean, and 17 water years within ±10% of the site mean annual precipitation (Figure S1). Further site details are summarised in Table 1.

We utilised the AmeriFlux BASE data product at 30-min temporal resolution excluding water years with data gaps larger than 60 days. Measurements used for analysis from these data products include precipitation (P), net longwave radiation, downwelling shortwave radiation, air pressure, relative humidity, air temperature, wind speed, and the latent heat flux measured by eddy covariance. For sites where atmospheric stability filtering was not previously applied (GLE, NR1, and MtB), a friction velocity (u*) threshold of 0.15 m s^{-1} was imposed to remove turbulent flux data during periods of insufficient turbulent mixing (e.g., Massman and Lee 2002; Blanken et al. 2009). This step was followed by gap-filling that used a moving median window approach with window lengths of 7, 28, and 60 days depending on gap size; More than 90% of data required only minor gap-filling with data gaps shorter than 7 days. Following the gap-filling procedure, 30-min data were aggregated to daily resolution to perform the calculations described below. A single exception for a large data gap in downwelling longwave radiation for MtB

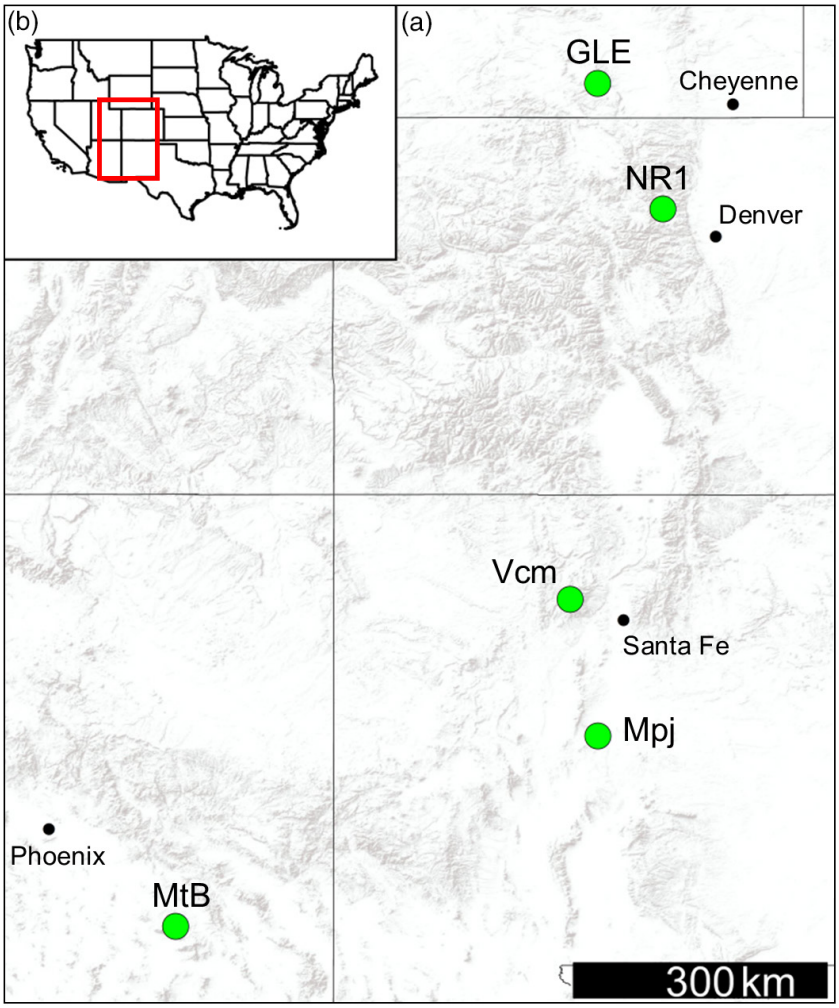

FIGURE 1 | (a) Map of the five study site locations and (b) the general location within the contiguous U.S.

was filled using linear interpolation considering the generally small variations in these data and the relatively small influence on subsequent calculations. For visualisation of the final daily dataset with gap-filled data indicated, see supplementary material (Figures S2–S6).

2.2 | Precipitation and Snow Data

Many of the sites did not have precipitation gauges equipped to obtain accurate measurements during freezing winter conditions. The precipitation gauges at GLE and Mpj, however, were determined to accurately measure winter P when corroborated with other nearby data sources such as SNOTEL or remote automated weather station (RAWS) that record precipitation and/or snow depth. To correct for the P gauge under catch at Vcm and MtB, correction factors were derived using average total water year p values at two nearby SNOTEL stations to estimate local P lapse rates with elevation for the water years observed. The P lapse rates were calculated by calculating the difference in water year P for each station and dividing by the elevation difference to determine the increase in precipitation with elevation. These lapse rates were then used to determine correction factors for each site based on the elevation difference between the sites and the reference precipitation gauge. These correction factors were then applied to a nearby US Climate Reference Network (CRN) gauge for Vcm and a RAWS for MtB (Table 1). For NR1, we used P data from a nearby CRN gauge located at a similar elevation as the flux tower. At each site, daily P data were used for the calculations described below. Further information pertaining to the additional meteorological stations utilised is available in the supplementary material (Table S1).

Snow depth data were obtained using a variety of sources and methods depending on data availability at each site. At GLE and NR1 we used data from the nearby Brooklyn Lake (367) and Niwot (633) SNOTEL sites, respectively. At Vcm, we used the Redondo RAWS site. Snow data are not collected near Mpj so snow depth was simulated using the SNOWPACK model (Lehning et al. 2002) forced with meteorological data from the site. The SNOWPACK simulations did not include canopy effects and the rain-snow threshold was modified to 2.5°C (Jennings et al. 2018). SNOWPACK has been previously used to accurately simulate snow accumulation and melt in continental montane environments (Lundy et al. 2001; Rutter et al. 2009; Webb et al. 2018). At all sites, snow depth data were used to determine dates for the start, peak, and end of the snow season. Due to some of the sites occasionally receiving shallow intermittent snow, the snow season was defined as requiring either a snow depth greater than 5 cm for a minimum of 7 days or a snowpack

TABLE 1 | Description of the study sites and key parameters used for calculations of years available during the 2014–2022 observation period. Sites are listed by latitude from north to south.

Site	Years	Elevation (m asl)	Vegetation functional type	Mean canopy height (m)	LAI (m^2/m^2)	Mean annual P (mm) [min / max]	Mean peak snow depth (cm) [date]	Mean first snow date [earliest / latest]	Mean snow off date [earliest / latest]	P station	P correction factor
GLE	2014–2020	3200	Evergreen Forest	7.0	2.6	1330 [1155 / 1645]	244 10-Apr	15-Oct [30-Sep / 20-Nov]	17-Jun [6-Jun / 29-Jun]	GLE	—
NR1	2014–2021	3050	Evergreen Forest	13.0	4.5	875 [690 / 1005]	148 4-Apr	20-Oct [30-Sep / 16-Nov]	4-Jun [22-May / 12-Jun]	CRN	—
Vcm	2015–2022	3030	Shrubland	1.0	1.7	840 [595 / 1075]	147 22-Feb	22-Nov [28-Oct / 10-Jan]	19-Apr [24-Mar / 26-May]	CRN	1.34
Mpj	2014–2022	2200	Woody Savanna	2.8	1.9	355 [290 / 405]	15 27-Dec	22-Dec [2-Nov / 28-Jan]	19-Jan [13-Nov / 20-Feb]	Mpj	—
MtB	2014–2021	2570	Evergreen Forest	10	4.6	915 [590 / 1490]	15 7-Jan	24-Dec [21-Nov / 24-Jan]	18-Feb [10-Jan / 13-Apr]	RAWS	1.27

that accumulates from multiple storm events (i.e., at least 24 h between depth increases).

2.3 | WAfR

We define WAfR in this study as the total amount of water available for downstream users including both natural and human systems. Thus, WAfR was calculated for each water year as total P minus total actual evapotranspiration (AET), which is equal to the sum of water year change in storage and streamflow. We calculated the total AET using the following equation:

$$\lambda E = \lambda_v \bullet \rho_w \bullet \mathrm{AET} \tag{1}$$

where λE is the latent heat flux measured by eddy covariance (e.g., Burba 2022), ρ_w is the density of water, and λ_v is the latent heat of vaporisation:

$$\lambda_v = 2.501 - 0.00236 \bullet T \tag{2}$$

where T is the observed near-surface air temperature. This approach to estimating WAfR accounts for changes in groundwater and soil moisture storage that may not be fully captured by a streamflow-based approach. The WAfR efficiency ($\mathrm{WAfR}_{\mathrm{eff}}$) was calculated as the total WAfR divided by the total P for each water year. Expected WAfR was also calculated using a Budyko-type approach (Berghuijs, Woods, and Hrachowitz 2014; Budyko 1974). The Budyko-type equation from Zhang, Dawes, and Walker (2001) was used to determine the expected AET/P ratio ($(\mathrm{AET/P})_{\mathrm{exp}}$) known as the evaporative index:

$$\left(\frac{\mathrm{AET}}{P}\right)_{\mathrm{exp}} = \frac{\left(1 + w \bullet \frac{\mathrm{PET}}{P}\right)}{\left[1 + w \bullet \left(\frac{\mathrm{PET}}{P}\right) + \left(\frac{\mathrm{PET}}{P}\right)^{-1}\right]} \tag{3}$$

where w is a fitting parameter and PET is potential evapotranspiration described in the next section. We used w for the southern Rocky Mountains (1.06) from Barnhart et al. (2016) to determine the expected evaporative index. Using the PET, AET, and p values for each water year, the Budyko-type WAfR anomaly (B_{anom}) was calculated as the expected evaporative index minus the observed evaporative index.

2.4 | Potential Evapotranspiration (PET)

PET calculations were performed using the Penman–Monteith approach (Monteith 1965):

$$\mathrm{PET} = \frac{\Delta \bullet \left[K_{\mathrm{in}} \bullet (1 - a) + L\right] + \rho_a \bullet c_p \bullet C_{\mathrm{at}} \bullet [e^* - e]}{\rho_w \bullet \lambda_v \bullet \left[\Delta + \gamma \bullet \left(1 + \frac{C_{at}}{C_{\mathrm{can}}}\right)\right]} \tag{4}$$

where Δ is the slope of the saturation vapour pressure–temperature relation at the observed air temperature, K_{in} is observed incoming shortwave radiation, α is the estimated ecosystem albedo (0.121 for Vcm and 0.062 for all other sites), L is observed net longwave radiation, ρ_a is observed air density, c_p is the specific heat of air, and C_{at} is atmospheric conductance

$(1/r_a)$, where r_a is the aerodynamic resistance, e^* is saturation vapour pressure for the observed air temperature, e is the observed vapour pressure, γ is the psychrometric constant, and C_{can} is canopy conductance. C_{at} is estimated as:

$$C_{at} = \frac{u_w}{6.25 \bullet \left[\ln\left(\frac{z_m - z_d}{z_0}\right)\right]^2} \quad (5)$$

where u_w is the measured wind speed, z_m is the height of wind speed measurements, z_d is the zero-plane displacement height estimated as 0.7 of the vegetation height, and z_0 is the roughness height estimated as 0.1 of the vegetation height.

C_{can} is estimated by Allen et al. (1989):

$$C_{can} = 0.5 \bullet \text{LAI} \bullet C_{leaf} \quad (5)$$

where LAI is the leaf area index and C_{leaf} is leaf conductance. LAI was estimated using MODIS data at each site location, averaging 3 values at the end of July or field measurements when available. For sites with coniferous trees, the one-sided MODIS LAI projection was doubled to account for the coniferous physiology of the needle leaf where stomata cover both sides (Frank et al. 2014; Knowles et al. 2023). We used the Stewart (1988) model for C_{leaf} assuming a maximum leaf conductance of $5\,\text{mm}\,\text{s}^{-1}$ and saturated soil.

The above-described methods were used to determine AET, AET/P, WAfR, WAfR_{eff}, and B_{anom} which were compared to the physical mechanisms. The methods for quantifying the physical mechanisms are described below.

2.5 | Physical Mechanisms

We focused on the three physical mechanisms that were recently identified as potential key contributors to snowmelt-driven runoff processes by Gordon et al. (2022): energy–water (EW) asynchrony, surface water input (SWI) intensity, and winter AET. EW asynchrony was determined by calculating the number of days between peak snowmelt and peak PET (Figure 2b). We chose to use PET rather than AET for this calculation due to the dependence of AET on available water in the system, as opposed to PET which is independent and more closely related to energy terms. Considering the snow season as previously described, peak snowmelt was defined as the median date from peak snow depth to zero snow depth to account for ecosystem-scale variation in snowmelt timing and/or rate due to differences in shading, slope aspect, and/or topography. Peak PET timing was defined as the date of maximum PET from a 10-day moving average of daily PET to account for inter- and intra-daily variability. The SWI intensity was calculated as the average amplitude of SWI events (i.e., snowmelt and rainfall; Figure 2a). For snowmelt events, a continuous melt "pulse" was considered as a single event or as multiple events if there was an observed pause where snow began accumulating for 1 day or more. Days with rain were treated as individual SWI events. The SWI intensity was calculated as total P divided by the number of SWI events for each water year. Thus, a site's theoretical maximum SWI intensity metric corresponds to a scenario in which the entirety of annual P occurs during winter producing a snowpack that continuously melts in spring, interpreted in this study as a more intense water input. Winter AET values were determined by summing observed daily water vapour fluxes during the winter season that we defined as January 1–March 31 of each water year.

2.6 | Statistical Analyses

To test the influence of the above-described individual physical mechanisms on WAfR metrics, regressions using the MATLAB curve fitting application were conducted with consideration of linear, exponential, and power functions. The best-fit regressions were determined based on the adjusted r^2 and root mean square error (RMSE) values. To analyse the influence of multiple mechanisms, stepwise linear and nonlinear regression models were evaluated utilising MATLAB's

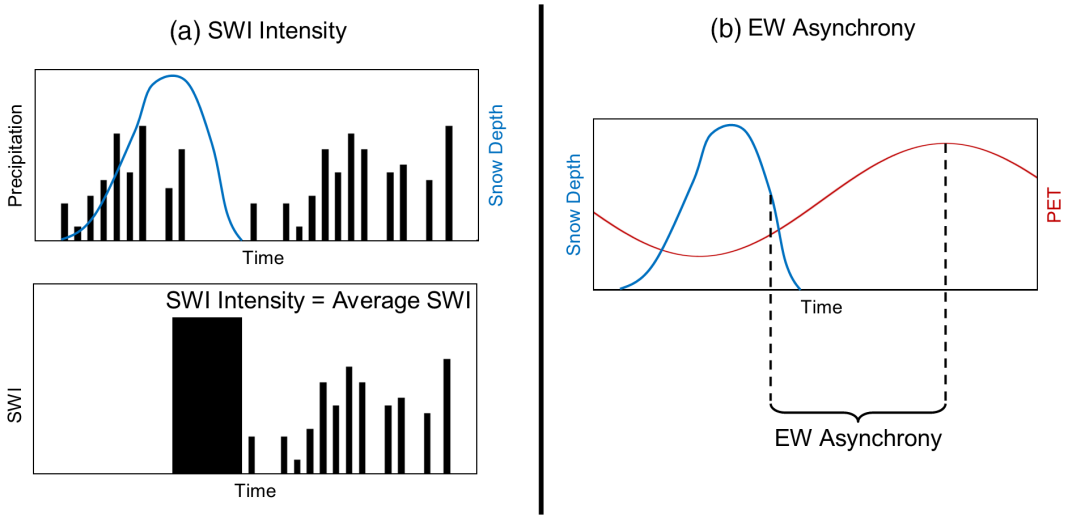

FIGURE 2 | Graphical representations of how (a) surface water input intensity (SWI) was defined as average SWI and (b) EW asynchrony (defined as the number of days between peak snowmelt and peak 10-day average PET) were calculated. Note axes are not to scale.

"stepwiselm" and "stepwisenlm" functions, respectively. The adjusted r^2, RMSE, and p values of the coefficients for each mechanism were used to evaluate the overall model fit and significance of terms.

3 | Results

A total of 39 water years were analysed with a similar number of years from each site (GLE = 7, NR1 = 8, Vcm = 8, Mpj = 9, MtB = 7). The sites provided a range of mean values for the physical mechanisms being investigated including EW asynchrony from 58 to 193 days (Figure 3a), SWI intensity from 2.6 to 37.3 mm (Figure 3b), and winter AET from 34 to 192 mm (Figure 3c). The hydroclimate of each site resulted in mean WAfR values from approximately 40 to 820 mm (Figure 3d), and mean $WAfR_{eff}$ values from 0.1 to 0.6 (Figure 3e), with GLE generally resulting in the highest values for both WAfR and $WAfR_{eff}$ and Mpj generally resulting in the lowest values except for MtB that showed the lowest single values of WAfR and $WAfR_{eff}$. There were only six water years with a negative B_{anom} and three of those years also had negative WAfR values (Figure 4). Overall, 10 of the 39 years were energy-limited with an aridity index (PET/P) less than 1.0, seven of which were observed at GLE (all data years) and three at Vcm.

3.1 | EW Asynchrony

The Mpj site had the highest EW asynchrony and NR1 had the lowest, although Vcm and GLE had similarly low values. When relating this physical mechanism to water balance terms and WAfR metrics, EW asynchrony showed the highest adjusted r^2 values for all regressions except the relationship with AET, where there was no significant relationship (Figure 5). Specifically, the magnitude of adjusted r^2 between EW asynchrony and AET/P and $WAfR_{eff}$ were similar (0.52) but signified opposing relationships with AET/P showing a positive correlation and $WAfR_{eff}$ showing a negative correlation to EW asynchrony. The correlation between EW

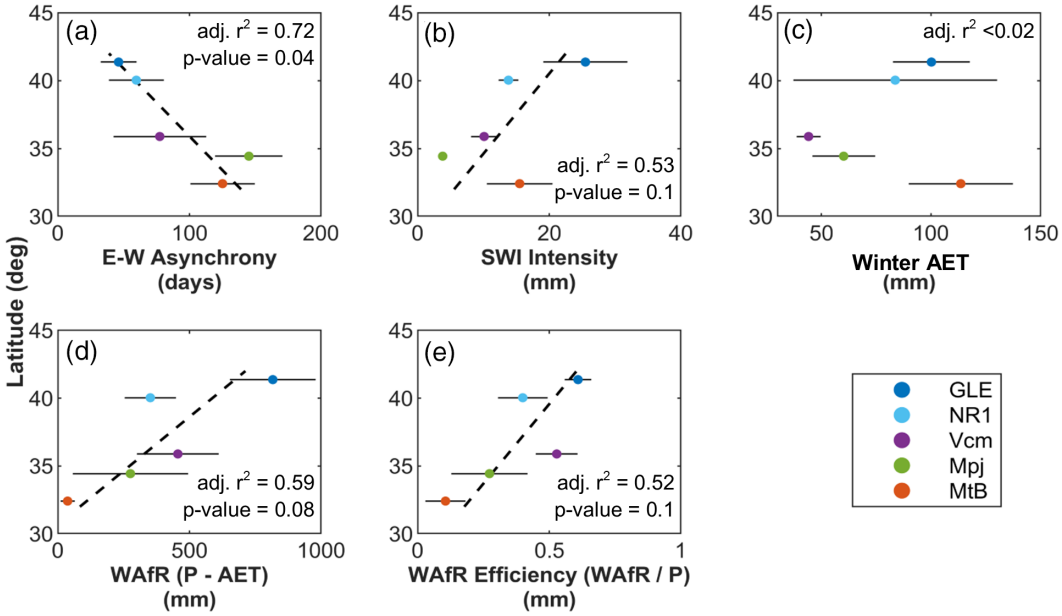

FIGURE 3 | Summary of physical mechanism and water available for runoff (WAfR) metric mean values for each site (bars indicate standard deviation) in relation to latitude. Panels show summaries for all observed water years including (a) EW asynchrony, (b) SWI intensity, (c) winter AET, (d) WAfR, and (e) $WAfR_{eff}$. Dashed lines indicate linear regressions when significant at the 0.1 level.

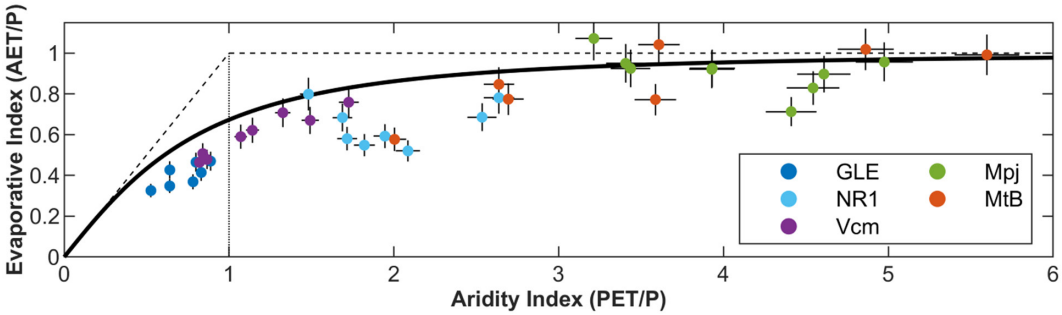

FIGURE 4 | Budyko-type plot for all water years analysed. Points represent individual water years and bars represent the estimated uncertainty using values from Knowles et al. (2015). The solid line represents the expected Budyko-type relationship from Equation (3) and the dashed lines represent physical limits to ET.

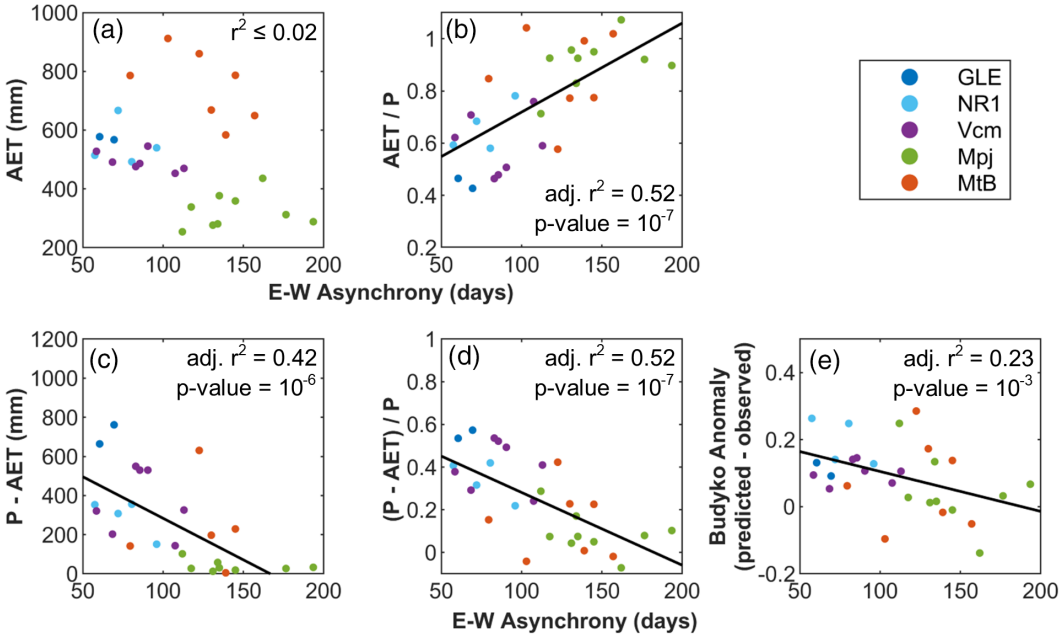

FIGURE 5 | EW asynchrony regression analyses for (a) AET, (b) evaporative index, (c) WAfR (P – AET), (d) $WAfR_{eff}$ ([P – AET] / P), and (e) B_{anom}. Solid lines correspond to the final regression equations with adjusted r^2 values shown for all, p values shown for linear functions, and function form with RMSE values indicated for nonlinear regression functions.

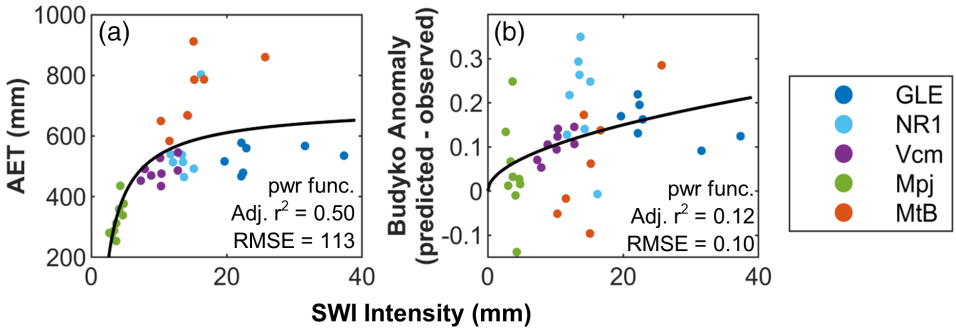

FIGURE 6 | SWI intensity regression analyses for (a) AET and (b) B_{anom}. Solid lines are used to display the final regression equations with function form, adjusted r^2 values, and RMSE shown.

asynchrony and WAfR was slightly lower (adjusted $r^2 = 0.42$) and in a negative direction (Figure 5b–d). Relative to other physical mechanisms, EW asynchrony was also most correlated with B_{anom} (adjusted $r^2 = 0.23$), showing a significant negative linear trend (Figure 5e).

3.2 | SWI Intensity

Mpj experienced all 9 of the lowest SWI intensity values, GLE experienced seven of the eight highest observed values, and MtB experienced the third highest observed value for 1 year. The correlation between SWI intensity and AET (adjusted $r^2 = 0.5$) was similar to the EW asynchrony regressions (Figure 6a), but the regression of SWI intensity and B_{anom} resulted in a lower adjusted r^2 value (0.12; Figure 6b). The relationships between both AET and B_{anom} to SWI intensity were positive in the form of power functions. The SWI intensity was only compared to AET and B_{anom} due to the occurrence of spurious correlation with the other metrics as a result of the shared P term (Kenney 1982; Brett 2004). In other words, while these regressions would likely result in high correlation values, mechanistic interpretation would not be possible.

3.3 | Winter AET

Winter AET had the most overlap across sites, but Vcm and NR1 experienced the lowest and highest observed values, respectively. Only AET was found to have a significant linear relationship (positive) with winter AET (adjusted $r^2 = 0.5$; $p << 0.01$; Figure 7a), and all other metrics were weakly correlated with adjusted r^2 values less than or equal to 0.02 (Figure 7b–e). Linear and nonlinear stepwise regressions did not improve model performance relative to basic regression analysis. As before, SWI intensity stepwise regressions were only performed with AET and B_{anom} as response variables to avert spurious conclusions.

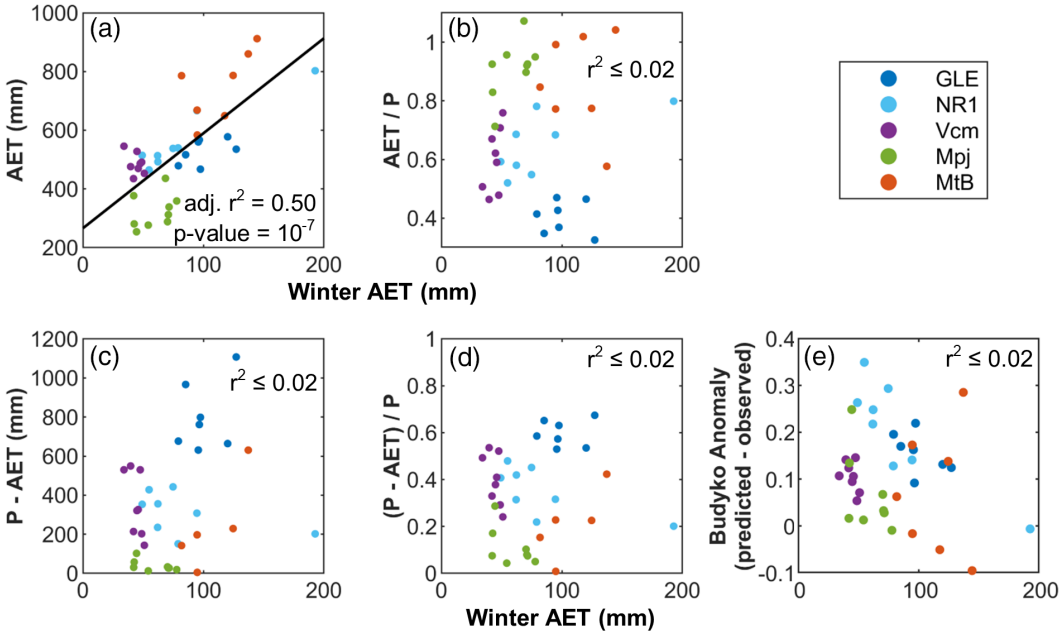

FIGURE 7 | Winter AET regression analyses for (a) annual AET, (b) evaporative index, (c) WAfR (P – AET), (d) $WAfR_{eff}$ ([P – AET] / P), and (e) B_{anom}. Adjusted r^2 values are shown for all panels with a solid line used to display the final regression along with the p value in panel (a).

4 | Discussion

Our study highlights the influence of physical mechanisms on WAfR across a range of hydroclimate conditions common to continental montane ecosystems. In addition, as hydroclimate shifts toward warmer and likely drier conditions, results from more southerly sites may be indicative of more northerly site dynamics in the future (Knowles et al. 2020). In this way, our southern sites Mpj and MtB showed greater EW asynchrony and less SWI intensity, resulting in reduced WAfR relative to northern sites in accordance with future projections (Figure 3a–d; e.g., Hale et al. 2023; Musselman et al. 2017). The most southerly site MtB, also experienced the greatest variability, particularly in annual WAfR and $WAfR_{eff}$, which may correspond to more variable intra-annual hydroclimate conditions (Figure 3). Moreover, the physical mechanisms correlated to WAfR variability were robust to disturbance level; the disturbed GLE and Vcm sites did not exhibit outlier behaviour in our analysis but grouped well with other sites. Thus, as continental montane forests increasingly establish new vegetation structures under warmer and/or drier conditions (e.g., Webb, Litvak, and Brooks 2023), WAfR may be expected to vary along the demonstrated relationships, although further research is necessary.

In comparison to other studies, our empirical findings present a slightly different perspective compared to recent modelling-focused investigations (e.g., Barnhart et al. 2016; Gordon et al. 2022). Specifically, our empirical results do not show a strong correlation between SWI intensity to B_{anom} as suggested by Barnhart et al. (2016), though we did not compare to other study parameters due to the potential for spurious correlation. Additionally, modelling efforts have suggested that EW asynchrony has the highest amount of variability in projected impacts and winter AET has the strongest relation to runoff (Gordon et al. 2022), whereas our empirical analysis in the Rocky Mountains found that winter AET was least correlated to WAfR, and EW asynchrony was the strongest predictor for water resources. However, it is important to note that the maximum adjusted r^2 was only 0.52 in the current study, suggesting more analyses are necessary to determine what factors may explain the remaining variability.

It is also important to note the uncertainty and limitations of our study. One limitation is that we only analysed five sites. While ecosystem scale observations such as those at AmeriFlux towers can offer insights, the sites used in this study may not represent other montane forests outside of the region. Although AmeriFlux towers are generally installed in locations that are thought to be representative, mountain ecosystems are heterogeneous, and complex terrain impacts water flow and vegetation growth (Chu et al. 2021), particularly following disturbance (e.g., Webb, Litvak, and Brooks 2023). Another potential source of uncertainty is forest structure. In particular, forest structure is known to influence snow accumulation, distribution, and melt, processes that relate to WAfR metrics. Lastly, we recognise that the WAfR metric may not translate to water available for use. WAfR is a combination of surface runoff and groundwater recharge, thus the groundwater system and its accessibility will be an important consideration when contextualising the present study with water resources. However, the spatial measurement footprint of AmeriFlux data offers general ecosystem scale observations that highlight where further investigation may be beneficial for eco-hydrological process understanding in montane forests.

Uncertainty in the measured variables also needs to be considered. We estimate the mean uncertainty of annual AET and winter AET for AmeriFlux sites to be 10% (e.g., Knowles et al. 2015). At Mpj 100% or more of winter precipitation was accounted for in AET due to the shallow intermittent

snowpack, but winter AET at all other sites, driven predominantly by snow sublimation, was between 10% and 46% with an average of 26% that compares well to other studies investigating sublimation in the Rocky Mountains (e.g., Knowles et al. 2015; Sexstone et al. 2018; Lundquist et al. 2024). The precipitation lapse rates for Vcm and MtB also include uncertainty. However, we conducted an analysis with ~80% reduction in Vcm and MtB P lapse rates, finding that r^2 values in our regression analysis increased by only 0.013 on average, and the significance of regressions remained unchanged. Therefore, the uncertainty in P lapse rates did not have a significant impact on results, although further research could improve estimates of local P lapse rates.

In continental montane forests, our results indicate that EW asynchrony has the strongest impact on all hydrological variables tested except for AET (Figure 5). However, while EW asynchrony showed a strong relationship with the evaporative index, it did not have a significant relationship with total AET. Furthermore, EW asynchrony maintained similar adjusted r^2 values when the fit to the evaporative index, WAfR and $WAfR_{eff}$ (0.52, 0.51 and 0.52, respectively), which may indicate that vegetation and root systems have adapted to thrive in the prevailing hydroclimate of each site and/or specific local conditions where critical zone structure and regular seasonal soil moisture patterns drive plant available water storage and its capacity (Martin et al. 2018). However, as EW asynchrony increases in the future from less snow accumulation and earlier snowmelt, WAfR and $WAfR_{eff}$ will decrease (Figure 5c) and montane forests will become increasingly moisture-stressed (e.g., Hale et al. 2023; Knowles et al. 2018), increasing the likelihood of severe disturbance (Abatzoglou and Williams 2016). Postdisturbance vegetation composition will subsequently correspond to new hydroclimate conditions and vary spatially depending on water distribution controlled by physiographic characteristics such as slope and aspect (Webb, Litvak, and Brooks 2023), potentially shifting systems along the regressions presented herein.

The SWI intensity was positively correlated (adj. $r^2 = 0.5$) with total water year AET, whereas EW asynchrony was not (Figure 6a), indicating that increased snowmelt intensity in spring months increased annual AET. No such relationship was characterised between EW asynchrony and annual AET. Given the influence of AET on WAfR, these results suggest a potentially important influence from SWI intensity, although future research to investigate connections between SWI intensity and water storage is needed to avoid spurious correlations. In particular, the underlying geology and critical zone structure are major determining factors of subsurface flow and storage dynamics (Brooks et al. 2015; Hammond et al. 2019) that link SWI intensity to streamflow and groundwater recharge (Barnhart et al. 2016). Higher SWI intensity is also related to deep snowpacks that can have different hydrologic flow paths during snowmelt relative to warmer, shallower snowpacks (Webb et al. 2020) in addition to deeper and colder snowpacks acting as additional storage reservoirs depending on the physiographic characteristics of the system (e.g., Katz et al. 2023; Webb et al. 2022).

Surprisingly, we observed that winter AET had no significant relationship to evaporative index, WAfR, $WAfR_{eff}$, or B_{anom} (Figure 7b–e). In fact, only AET showed a significant relationship with winter AET (Figure 7a), resulting in an adjusted r^2 of 0.50 that was similar to the other significant relationships that were characterised. This may be due to snowpack dynamics (Table 1) where the northern, colder sites have more mobile snow (promoting sublimation) from both tree canopies and blowing surface snow (Sexstone et al. 2018) that creates a greater surface area exposed to the atmosphere (Frank et al. 2019; Knowles et al. 2023), whereas warmer snowpacks experience more melt-freeze cycles (Sturm and Liston 2021), promoting surface crusts that are less prone to wind transportation and the resulting sublimation (Vionnet et al. 2013) that results in more snowmelt infiltration relative to snowfall. However, winter AET occasionally exceeded winter P at the more southerly sites, indicating a likely increased contribution of soil moisture and groundwater storage to winter AET (Brooks et al. 2015; Tai et al. 2021). As continental montane forests shift toward increasingly warmer and shallower snowpacks, winter vapour flux sources are likely to change, resulting in poor direct relationships to the WAfR metrics analysed in this study. Additionally, water vapour fluxes may be reduced from sites that experience forest canopy loss due to disturbance (Frank et al. 2019), raising the question as to how disturbance and climatic processes will compound to impact site-specific winter AET-WAfR relationships.

Regression analysis of physical mechanisms and B_{anom} did not yield high correlations. This is particularly interesting considering the number of studies that have characterised Budyko-type relationships in continental, montane forests (e.g., Barnhart et al. 2016; Berghuijs, Woods, and Hrachowitz 2014; Knowles et al. 2015). Here we note that the Budyko-type framework assumes no change in, or influence from, groundwater storage, which can have significant impacts on hydrological processes (Brooks et al. 2021; Wolf et al. 2023). Furthermore, the choice of PET equations could affect Budyko-type analyses when sites such as GLE have ~50% of total annual water vapour loss sourced from a winter snowpack (Frank et al. 2019; Schlaepfer et al. 2014). It is also important to note that a recent analysis of Budyko-type framework equations indicated that fitting parameters may be nonunique and not reflective of the dynamic behaviour of individual systems (Reaver et al. 2022). Taken together, a combination of storage and/or fitting parameters may explain the lower r^2 values between B_{anom} and the physical mechanisms evaluated herein.

The current results constrain the mechanisms driving variability in WAfR metrics and their relative significance. Our empirical analysis shows the strong influence of EW asynchrony on WAfR and $WAfR_{eff}$ in addition to the strong influence of SWI intensity on AET. The strong influence of EW asynchrony underscores the importance of snowmelt timing for water resources, highlighting the importance of accurately computing the snowpack energy balance for modelling studies. Our study also addresses and highlights a need for empirical analyses given (1) the currently changing conditions in mid-latitude montane systems globally where (2) WAfR has been linked to multi-year time-scale patterns of groundwater storage and baseflow (Brooks et al. 2021). As a result, we advocate for including variable interannual hydrologic storage components (i.e., groundwater and soil moisture) in future

empirical research and hydrological modelling efforts in order to improve predictive capabilities for runoff and WAfR forecasting efforts. In general, the current results broadly support a need for novel metrics that are appropriate for hydrological systems where stationarity no longer exists (Milly et al. 2008; Yang et al. 2021).

5 | Conclusions

We quantified the influence of physical mechanisms related to variability in snowpack conditions on WAfR in mid-latitude, and continental montane regions. The north–south transect of sites resulted in a hydroclimatic gradient that yielded process-based insights into how hydroclimate drives variability in WAfR. Among the three physical mechanisms tested, energy-water asynchrony best predicted system efficiency for WAfR (adjusted $r^2 = 0.52$), with similar r^2 values for the evaporative index. In contrast, SWI intensity was a significant predictor (adjusted $r^2 = 0.50$) of total evapotranspiration, but energy-water asynchrony was not. Budyko-type anomalies were not well predicted by the mechanisms tested in this study. These results highlight the importance of snowmelt timing in determining WAfR in mid-latitude, continental montane forests.

Acknowledgements

We would like to acknowledge the University of Wyoming Department of Civil and Architectural Engineering and Construction Management for supporting R. Webb in teaching the advanced hydrology class that led to this paper. A semester-long course project determined the physical mechanisms and metrics analysed in this study. We would also like to express our appreciation to anonymous reviewers and Jessica Lundquist for constructive feedback that improved the final version of this paper.

Data Availability Statement

AmeriFlux BASE data may be accessed through the online repository (https://AmeriFlux.lbl.gov/data/download-data/). SNOTEL historical data for the sites may be accessed through the USDA NRCS National Water and Climate Center website (https://wcc.sc.egov.usda.gov/nwcc/tabget). CRN precipitation data may be accessed through NOAA (https://www.ncei.noaa.gov/access/crn/qcdatasets.html). RAWS data may be accessed through the Desert Research Institute (https://raws.dri.edu/).

References

Abatzoglou, J. T., and A. P. Williams. 2016. "Impact of Anthropogenic Climate Change on Wildfire Across Western US Forests." *Proceedings of the National Academy of Sciences of the United States of America* 113: 11770–11775. https://doi.org/10.1073/pnas.1607171113.

Adam, J. C., A. F. Hamlet, and D. P. Lettenmaier. 2009. "Implications of Global Climate Change for Snowmelt Hydrology in the Twenty-First Century." *Hydrological Processes* 23, no. 7: 962–972.

Allen, R. G., M. E. Jensen, J. L. Wright, and R. D. Burman. 1989. "Operational Estimates of Reference Evapotranspiration." *Agronomy Journal* 81, no. 4: 650–662.

Bales, R. C., N. P. Molotch, T. H. Painter, M. D. Dettinger, R. Rice, and J. Dozier. 2006. "Mountain Hydrology of the Western United States." *Water Resources Research* 42, no. 8: W08432.

Barnhart, T., N. Molotch, B. Livneh, A. Harpold, J. Knowles, and D. Schneider. 2016. "Snowmelt Rate Dictates Streamflow." *Geophysical Research Letters* 43, no. 15: 8006–8016.

Barron-Gafford, G. 2022. "AmeriFlux BASE US-MtB Mt Bigelow, Ver. 4-5." AmeriFlux AMP, BASE dataset.

Berghuijs, W., R. Woods, and M. Hrachowitz. 2014. "A Precipitation Shift From Snow Towards Rain Leads to a Decrease in Streamflow." *Nature Climate Change* 4, no. 7: 583–586.

Blanken, P. D., M. W. Williams, S. P. Burns, et al. 2009. "A Comparison of Water and Carbon Dioxide Exchange at a Windy Alpine Tundra and Subalpine Forest Site Near Niwot Ridge, Colorado." *Biogeochemistry* 95: 61–76. https://doi.org/10.1007/s10533-009-9325-9.

Blanken, P. D., R. K. Monson, S. P. Burns, D. R. Bowling, and A. A. Tunispeed. 2022. "AmeriFlux BASE US-NR1 Niwot Ridge Forest (LTER NWT1), Ver. 19-5." AmeriFlux AMP, BASE dataset.

Brett, M. T. 2004. "When is a Correlation Between Non-Independent Variables "Spurious?"." *Oikos* 105: 647–656. https://doi.org/10.1111/j.0030-1299.2004.12777.x.

Brooks, P. D., A. Gelderloos, M. A. Wolf, et al. 2021. "Groundwater-Mediated Memory of Past Climate Controls Water Yield in Snowmelt-Dominated Catchments." *Water Resources Research* 57, no. 10: e2021WR030605.

Brooks, P., J. Chorover, Y. Fan, et al. 2015. "Hydrological Partitioning in the Critical Zone: Recent Advances and Opportunities for Developing Transferable Understanding of Water Cycle Dynamics." *Water Resources Research* 51, no. 9: 6973–6987.

Budyko, M. I. 1974. *Climate and Life*. New York: Academic Press.

Burba, G. 2022. *Eddy Covariance Method for Scientific, Regulatory, and Commercial Applications*. Lincoln: LI-COR Biosciences. ISBN 978-0-578-97714-0.

Chu, H., X. Luo, Z. Ouyang, et al. 2021. "Representativeness of Eddy-Covariance Flux Footprints for Areas Surrounding AmeriFlux Sites." *Agricultural and Forest Meteorology* 301: 108350. https://doi.org/10.1016/j.agrformet.2021.108350.

Frank, J. M., W. J. Massman, B. E. Ewers, and D. G. Williams. 2019. "Bayesian Analyses of 17 Winters of Water Vapor Fluxes Show Bark Beetles Reduce Sublimation." *Water Resources Research* 55, no. 2: 1598–1623.

Frank, J. M., W. J. Massman, B. E. Ewers, L. S. Huckaby, and J. F. Negrón. 2014. "Ecosystem CO_2/H_2O Fluxes Are Explained by Hydraulically Limited Gas Exchange During Tree Mortality From Spruce Bark Beetles." *Journal of Geophysical Research: Biogeosciences* 119, no. 6: 1195–1215.

Frank, J., and B. Massman. 2021. "AmeriFlux BASE US-GLE GLEES, Ver. 8-5." AmeriFlux AMP, BASE dataset.

Gordon, B. L., P. D. Brooks, S. A. Krogh, et al. 2022. "Why Does Snowmelt-Driven Streamflow Response to Warming Vary? A Data-Driven Review and Predictive Framework." *Environmental Research Letters* 17, no. 5: 053004. https://doi.org/10.1088/1748-9326/ac64b4.

Hale, K. E., K. S. Jennings, K. N. Musselman, B. Livneh, and N. P. Molotch. 2023. "Recent Decreases in Snow Water Storage in Western North America." *Communications Earth & Environment* 4, no. 1: 170.

Hammond, J. C., A. A. Harpold, S. Weiss, and S. K. Kampf. 2019. "Partitioning Snowmelt and Rainfall in the Critical Zone: Effects of Climate Type and Soil Properties." *Hydrology and Earth System Sciences Discussions* 23, no. 9: 3553–3570.

Hammond, J. C., and S. K. Kampf. 2020. "Subannual Streamflow Responses to Rainfall and Snowmelt Inputs in Snow-Dominated Watersheds of the Western United States." *Water Resources Research* 56, no. 4: e2019WR026132.

Harpold, A., P. Brooks, S. Rajagopal, I. Heidbuchel, A. Jardine, and C. Stielstra. 2012. "Changes in Snowpack Accumulation and Ablation in the Intermountain West." *Water Resources Research* 48, no. 11: W11501.

Immerzeel, W. W., A. F. Lutz, M. Andrade, et al. 2020. "Importance and Vulnerability of the World's Water Towers." *Nature* 577, no. 7790: 364–369.

IPCC. 2022. "Climate Change 2022: Impacts, Adaptation, and Vulnerability." In *Contribution of Working Group II to the Sixth Assessment Report of the Intergovernmental Panel on Climate Change*, edited by H.-O. Pörtner, D. C. Roberts, M. Tignor, E. S. Poloczanska, K. Mintenbeck, A. Alegría, M. Craig, S. Langsdorf, S. Löschke, V. Möller, A. Okem, and B. Rama, 3056. Cambridge, UK and New York, NY, USA: Cambridge University Press. https://doi.org/10.1017/9781009325844.

Jennings, K., T. Winchell, B. Livneh, and N. Molotch. 2018. "Spatial Variation of the Rain-Snow Temperature Threshold Across the Northern Hemisphere." *Nature Communications* 9: 1148.

Katz, L., G. Lewis, S. Krogh, et al. 2023. "Antecedent Snowpack Cold Content Alters the Hydrologic Response to Extreme Rain-On-Snow Events." *Journal of Hydrometeorology* 24: 1825–1846. https://doi.org/10.1175/JHM-D-22-0090.1.

Kenney, B. C. 1982. "Beware of Spurious Self-Correlations!" *Water Resources Research* 18, no. 4: 1041–1048. https://doi.org/10.1029/WR018i004p01041.

Kim, R. S., S. Kumar, C. Vuyovich, et al. 2021. "Snow Ensemble Uncertainty Project (SEUP): Quantification of Snow Water Equivalent Uncertainty Across North America via Ensemble Land Surface Modelling." *Cryosphere* 15, no. 2: 771–791.

Kirchner, J. 2006. "Getting the Right Answers for the Right Reasons: Linking Measurements, Analyses, and Models to Advance the Science of Hydrology." *Water Resources Research* 42: W03S04. https://doi.org/10.1029/2005WR004362.

Knowles, J. F., N. P. Molotch, E. Trujillo, and M. E. Litvak. 2018. "Snowmelt-Driven Trade-Offs Between Early and Late Season Productivity Negatively Impact Forest Carbon Uptake During Drought." *Geophysical Research Letters* 45: 3087–3096. https://doi.org/10.1002/2017GL076504.

Knowles, J. F., N. R. Bjarke, A. M. Badger, et al. 2023. "Bark Beetle Impacts on Forest Evapotranspiration and Its Partitioning." *Science of the Total Environment* 880: 163260.

Knowles, J. F., R. L. Scott, J. A. Biederman, et al. 2020. "Montane Forest Productivity Across a Semiarid Climatic Gradient." *Global Change Biology* 26, no. 12: 6945–6958.

Knowles, J., A. Harpold, R. Cowie, et al. 2015. "The Relative Contributions of Alpine and Subalpine Ecosystems to the Water Balance of a Mountainous, Headwater Catchment." *Hydrological Processes* 29, no. 22: 4794–4808.

Knowles, N., M. Dettinger, and D. Cayan. 2006. "Trends in Snowfall Versus Rainfall in the Western United States." *Journal of Climate* 19, no. 18: 4545–4559.

Lehning, M., P. Bartelt, B. Brown, C. Fierz, and P. Satyawali. 2002. "A Physical SNOWPACK Model for the Swiss Avalanche Warning: Part II. Snow Microstructure." *Cold Regions Science and Technology* 35, no. 3: 147–167.

Li, D., M. Wrzesien, M. Durand, J. Adam, and D. Lettenmaier. 2017. "How Much Runoff Originates as Snow in the Western United States, and How Will That Change in the Future?" *Geophysical Research Letters* 44, no. 12: 6163–6172.

Litvak, M. 2023a. "AmeriFlux BASE US-Mpj Mountainair Pinyon-Juniper Woodland, Ver. 21-5, AmeriFlux AMP, BASE dataset."

Litvak, M. 2023b. "AmeriFlux BASE US-Mpj Mountainair Pinyon-Juniper Woodland, Ver. 21-5." AmeriFlux AMP, BASE dataset.

Lundquist, J. D., J. Vano, E. Gutmann, et al. 2024. "Sublimation of Snow." *Bulletin of the American Meteorological Society* 105: E975–E990. https://doi.org/10.1175/BAMS-D-23-0191.1.

Lundy, C., R. Brown, E. Adams, K. Birkeland, and M. Lehning. 2001. "A Statistical Validation of the Snowpack Model in a Montana Climate." *Cold Regions Science and Technology* 33, no. 2–3: 237–246.

Mankin, J., D. Viviroli, D. Singh, A. Hoekstra, and N. Diffenbaugh. 2015. "The Potential for Snow to Supply Human Water Demand in the Present and Future." *Environmental Research Letters* 10, no. 11: 114016.

Martin, J., N. Looker, Z. Hoylman, K. Jencso, and J. Hu. 2018. "Differential Use of Winter Precipitation by Upper and Lower Elevation Douglas Fir in the Northern Rockies." *Global Change Biology* 24, no. 12: 5607–5621. https://doi.org/10.1111/gcb.14435.

Massman, W. J., and X. Lee. 2002. "Eddy Covariance Flux Corrections and Uncertainties in Long-Term Studies of Carbon and Energy Exchanges." *Agricultural and Forest Meteorology* 113: 121–144. https://doi.org/10.1016/S0168-1923(02)00105-3.

McCabe, G. J., D. M. Wolock, and M. Valentin. 2018. "Warming Is Driving Decreases in Snow Fractions While Runoff Efficiency Remains Mostly Unchanged in Snow-Covered Areas of the Western United States." *Journal of Hydrometeorology* 19, no. 5: 803–814.

Milly, P. C. D., J. Betancourt, M. Falkenmark, et al. 2008. "Stationarity Is Dead: Whither Water Management?" *Science* 319, no. 5863: 573–574.

Milly, P. C. D., J. Kam, and K. A. Dunne. 2018. "On the Sensitivity of Annual Streamflow to Air Temperature." *Water Resources Research* 54, no. 4: 2624–2641.

Monteith, J. L. 1965. "Evaporation and Environment." Paper Presented at Proceedings of the 19th Symposium of the Society for Experimental Biology, Cambridge University Press.

Musselman, K., M. Clark, C. Liu, K. Ikeda, and R. Rasmussen. 2017. "Slower Snowmelt in a Warmer World." *Nature Climate Change* 7, no. 3: 214–219.

Raleigh, M. S., C. C. Landry, M. Hayashi, W. L. Quinton, and J. D. Lundquist. 2013. "Approximating Snow Surface Temperature From Standard Temperature and Humidity Data: New Possibilities for Snow Model and Remote Sensing Evaluation." *Water Resources Research* 49, no. 12: 8053–8069.

Reaver, N. G. F., D. A. Kaplan, H. Klammler, and J. W. Jawitz. 2022. "Theoretical and Empirical Evidence Against the Budyko Catchment Trajectory Conjecture." *Hydrology and Earth System Sciences* 26, no. 5: 1507–1525.

Running, S. W., D. D. Baldocchi, D. P. Turner, S. T. Gower, P. S. Bakwin, and K. A. Hibbard. 1999. "A Global Terrestrial Monitoring Network Integrating Tower Fluxes, Flask Sampling, Ecosystem Modeling and EOS Satellite Data." *Remote Sensing of Environment* 70, no. 1: 108–127. https://doi.org/10.1016/S0034-4257(99)00061-9.

Rutter, N., R. Essery, J. Pomeroy, et al. 2009. "Evaluation of Forest Snow Processes Models (SnowMIP2)." *Journal of Geophysical Research-Atmospheres* 114: D06111. https://doi.org/10.1029/2008JD011063.

Schlaepfer, D. R., B. E. Ewers, B. N. Shuman, et al. 2014. "Terrestrial Water Fluxes Dominated by Transpiration: Comment." *Ecosphere* 5, no. 5: art61.

Sexstone, G. A., D. W. Clow, S. R. Fassnacht, et al. 2018. "Snow Sublimation in Mountain Environments and Its Sensitivity to Forest Disturbance and Climate Warming." *Water Resources Research* 54, no. 2: 1191–1211.

Stewart, J. B. 1988. "Modelling Surface Conductance of Pine Forest." *Agricultural and Forest Meteorology* 43, no. 1: 19–35.

Sturm, M., and G. E. Liston. 2021. "Revisiting the Global Seasonal Snow Classification: An Updated Dataset for Earth System Applications." *Journal of Hydrometeorology* 22, no. 11: 2917–2938.

Sturm, M., M. Goldstein, and C. Parr. 2017. "Water and Life From Snow: A Trillion Dollar Science Question." *Water Resources Research* 53, no. 5: 3534–3544.

Tai, X., M. D. Venturas, D. S. Mackay, P. D. Brooks, and L. B. Flanagan. 2021. "Lateral Subsurface Flow Modulates Forest Mortality Risk to Future Climate and Elevated CO_2." *Environmental Research Letters* 16, no. 8: 084015.

Vano, J. A., B. Udall, D. R. Cayan, et al. 2014. "Understanding Uncertainties in Future Colorado River Streamflow." *Bulletin of the American Meteorological Society* 95, no. 1: 59–78.

Vionnet, V., G. Guyomarc'h, F. Naaim Bouvet, et al. 2013. "Occurrence of Blowing Snow Events at an Alpine Site Over a 10-Year Period: Observations and Modelling." *Advances in Water Resources* 55: 53–63.

Webb, R. W., K. Jennings, M. Fend, and N. Molotch. 2018. "Combining Ground Penetrating Radar With Terrestrial LiDAR Scanning to Estimate the Spatial Distribution of Liquid Water Content in Seasonal Snowpacks." *Water Resources Research* 54: 10339–10349.

Webb, R. W., K. N. Musselman, S. Ciafone, K. E. Hale, and N. P. Molotch. 2022. "Extending the Vadose Zone: Characterizing the Role of Snow for Liquid Water Storage and Transmission in Streamflow Generation." *Hydrological Processes* 36, no. 3: e14541.

Webb, R. W., M. E. Litvak, and P. D. Brooks. 2023. "The Role of Terrain-Mediated Hydroclimate in Vegetation Recovery After Wildfire." *Environmental Research Letters* 18, no. 6: 064036.

Webb, R. W., O. Wigmore, K. Jennings, M. Fend, and N. P. Molotch. 2020. "Hydrologic Connectivity at the Hillslope Scale Through Intra-Snowpack Flow Paths During Snowmelt." *Hydrological Processes* 34, no. 7: 1616–1629.

Wolf, M. A., L. R. Jamison, D. K. Solomon, C. Strong, and P. D. Brooks. 2023. "Multi-Year Controls on Groundwater Storage in Seasonally Snow-Covered Headwater Catchments." *Water Resources Research* 59, no. 6: e2022WR033394.

Yang, Y., M. L. Roderick, D. Yang, et al. 2021. "Streamflow Stationarity in a Changing World." *Environmental Research Letters* 16, no. 6: 064096.

Zhang, L., W. R. Dawes, and G. R. Walker. 2001. "Response of Mean Annual Evapotranspiration to Vegetation Changes at Catchment Scale." *Water Resources Research* 37, no. 3: 701–708.

Supporting Information

Additional supporting information can be found online in the Supporting Information section.